Published in final edited form as:
Proc SPIE. 2013 March 13; 8669: . doi:10.1117/12.2006490.

Automatic Segmentation of Right Ventricle on Ultrasound Images Using Sparse Matrix Transform and Level Set

Xulei Qin[1], **Zhibin Cong**[1], **Luma V. Halig**[1], and **Baowei Fei**[1,2,3,*]

[1]Department of Radiology and Imaging Sciences, Emory University, Atlanta, GA

[2]Department of Mathematics and Computer Science, Emory University, Atlanta, GA

[3]Department of Biomedical Engineering, Emory University and Georgia Institute of Technology

Abstract

An automatic framework is proposed to segment right ventricle on ultrasound images. This method can automatically segment both epicardial and endocardial boundaries from a continuous echocardiography series by combining sparse matrix transform (SMT), a training model, and a localized region based level set. First, the sparse matrix transform extracts main motion regions of myocardium as eigenimages by analyzing statistical information of these images. Second, a training model of right ventricle is registered to the extracted eigenimages in order to automatically detect the main location of the right ventricle and the corresponding transform relationship between the training model and the SMT-extracted results in the series. Third, the training model is then adjusted as an adapted initialization for the segmentation of each image in the series. Finally, based on the adapted initializations, a localized region based level set algorithm is applied to segment both epicardial and endocardial boundaries of the right ventricle from the whole series. Experimental results from real subject data validated the performance of the proposed framework in segmenting right ventricle from echocardiography. The mean Dice scores for both epicardial and endocardial boundaries are 89.1%±2.3% and 83.6±7.3%, respectively. The automatic segmentation method based on sparse matrix transform and level set can provide a useful tool for quantitative cardiac imaging.

Keywords

Image segmentation; ultrasound imaging; sparse matrix transform; level set; right ventricle; cardiac imaging; heart; myocardium; genetic algorithm; functional imaging

1. INTRODUCTION

Reliable evaluation of the structure and function of heart ventricles from echocardiographic images is an important issue for clinical examination and diagnosis. Various methods were proposed to segment the left ventricle (LV) structures. For example, active shape model was widely used in this area [1]. However, it was difficult to directly segment the LV structures without any model constraint. Therefore, shape prior was introduced in order to improve the performance, such as the use of training shape model contours to segment the LV epicardial boundary [2] and the application of ellipse shape models to constrain the short axis for LV

*Corresponding author: baowei.fei@emory.edu; Website: www.feilab.org.

border detection [3]. Especially, wall thickness constraint was introduced to detect both endocardial and epicardial boundaries, which were applied to both 2D and 3D echocardiography segmentations [4, 5]. Meanwhile, other efforts were made for the automatic segmentation of LV boundaries from echocardiography. Statistical approaches such as principal component analysis (PCA) based training model [6, 7], boosted shape detection methods [8], and the use of pre-intensity distributions in images [4]or radiofrequency (RF) data [9] were applied for this purpose.

Although various methods have been applied to segment the LV images, they cannot be directly applied to segment right ventricle (RV) on echocardiography because of two additional problems: (i) poor imaging quality for RV and (ii) irregular geometry of the RV. Despite the importance of its structure evaluations for clinical diagnosis, RV is often segmented manually by experts, which is time consuming because hundreds of images in one image series need to be segmented and also because the irregular shape of RV makes the segmentation difficult. Therefore, we propose an automatic segmentation framework to segment RV from echocardiographic series, which combines sparse matrix transform (SMT), training models, and a level set algorithm.

2. METHODS

The proposed framework contains the training and application stages. Firstly, 450 images from 9 different echocardiographic series were used to generate the training model. Both epicardial and endocardial boundaries of RV have been manually defined by a cardiologist (ZC). Based on the expert's results, a training model was built by the SMT method. After building the training model, the RV myocardium can be extracted from a new series of echocardiography in the next application stage. During this stage, the SMT method is used to extract the eigenimages from the whole series. After that, the main RV region and the transformation relationship to the training model are calculated by a registration process. Based on these results, initialization regions for each image in the current series can be decided by adapting the shape of the training model. Subsequently, based on the initialization, RV myocardium in each image is segmented by a localized region based level set algorithm, which is proved suitable for myocardium segmentation [5]. Figure 1 shows the flowchart of the segmentation framework.

2.1 SMT eigenimages and registration

SMT has been successfully applied in the face recognition area [10]. Comparing with other methods such as PCA, SMT has several useful advantages: first, it can improve the accuracy of the eigen-decomposition, particularly when the number of observations is less than the vector dimension; second, it is computationally fast to apply the resulting SMT eigen-decomposition. Moreover, a graph based SMT is able to estimate the eigenimages due to the graphical constraint [11]. Furthermore, SMT needs less sample data and make it possible to analyze the echocardiographic series, which contains much less sample data than the image dimension.

SMT extracts the myocardium regions with most motion as eigenimages, which can neglect other stable structures of non-myocardial regions, such as apex part, as shown in Figure 2(b) and (c). Because the RV shape is different from other structures, such as atriums and left ventricle, it can be easily extracted from the SMT eigenimages by registering it with the mean shape of the training model (Figure 2(e)) [12, 13]. The transformation parameters such as rotation, shift and scaling, will be applied to the following adapted initialization step in order to adjust the training model. Meanwhile, this extracted RV shape indicates the most probable location of the RV in the whole series, which will restrict the searching region

during the adapted initialization, and thus reduce the calculation time of the SMT training model and also keep the model variance in a reasonable region.

Moreover, these results will be more robust than just directly adapting training models to each image because the SMT synthesizes the whole series information and reduces the effects of poor-quality imaging, such as image regions with missing crucial structures or bright noise. Similar to the situation that a cardiologist uses the dynamic images of echocardiography rather than only one static image frame to detect the shape and location of RV in the clinic, the approach based on SMT and training model is to simulate this human recognition process for automatic segmentation.

2.2 Adapted initialization and level set segmentation

The training data of inner and outer boundaries of the RV myocardium is processed by the SMT method. During the application stage, the most similar shape of the training model to the RV structure in each image is chosen by adapting the weight parameters in their searching space, which is the initialization for the following level set segmentation [14, 15].

$$S=\bar{\mathrm{s}}+\sum_{i=1}^{k} b_i \times U_i, \quad (1)$$

Where $s\bar{}$ is the mean shape of the training model, U_i are the eigen-vectors, b_i is the weight parameters related to eigen-values.

The correct initialization and shape prior constraints are important for the level set segmentation because the contours can leak out from weak boundaries, especially for RV regions that can have missing boundaries. The criteria to choose the best parameters of the training model follow the mean separation energy function:

$$E_{ms}=-\frac{1}{2}(u-v)^2, \quad (2)$$

where u and v are the mean intensities in and outside of the ROI, respectively. After the adapted step, each image has an initialization mask for the level set segmentation.

The gray region in Figure 2(e), which is the RV myocardium, corresponds to the negative level set, and its epicardial and endocardial boundaries correspond to the zero level set. This localized region based level set framework has been applied to the LV myocardium segmentation using the method as previously reported [5, 16]. Similarly, our level set function also contains three aspects: image data, shape prior, and thickness constraint. The mean separation energy is also applied to calculate the image data energy. The initialization mask is not only used as initialization but also as the shape prior. The energy calculation is designed as followed:

$$E=E_{image}(\varphi, I, H_T)+\lambda E_{shape}(\varphi, S, I, H_T), \quad (3)$$

Here, I is the image data, S is the model shape data, λ is a weighted parameter. During the curve evolution to minimize the energy function E, E_{image} tends to make E as small as possible when evolution nearer to the region edges. On the contrary, E_{shape} makes E as big as possible during the evolution farther from its original position. The thickness constraint H_T is defined as a Heaviside function:

$$H_T(\varphi(\bar{x}+\bar{N}\cdot R_T))=\begin{cases}1, & \varphi>0\\ 0, & otherwise\end{cases}, \quad (4)$$

Where R_T is the distance between epicardial and endocardial boundaries at the zero level set point and N is the inward normal of a point x. The thickness constraint keeps the minimal thickness between both boundaries more than an average value, such as 10 pixels here.

2.3 Segmentation evaluation

Quantitative performance assessment of the method was conducted by comparing the automatic segmentation results with the corresponding gold standard data from manual segmentation by a cardiologist. Various methods were used for the evaluation of segmentation and registration [17–26]. In this study, the Dice similarity was used as the performance assessment metrics in myocardium segmentation. The Dice similarity was computed as follows:

$$Dice(S,G)=\frac{2Area(S\cap G)}{Area(S)+Area(G)}, \quad (3)$$

where S and G represent the pixel set of the RV segmentation regions obtained by the algorithm and gold standard data, respectively.

3. RESULTS

The method was evaluated by eight echocardiography randomly selected from different subjects' database, totally containing 400 images. Both the epicardial and endocardial Dice scores are shown in Table 1, which are 89.1%±2.3% and 83.6±7.3%, respectively. The endocardial Dice scores are lower than epicardial ones because the endocardial region is smaller and more irregular than the epicardial regions, especially in the apical regions. Moreover, the papillary tissues also affect the endocardial segmentation accuracy for both manual and automatic results.

Figure 3 illustrates the results segmented by three different frameworks where the green solid lines are the detected boundaries of myocardium: (i) a general localized level set segmentation without adapted initialization, (ii) a localized level set segmentation with an adapted initialization rather than any shape constraint, and (iii) our proposed one with the adapted initialization and also the shape constraint. The result segmented by our framework is compared with the corresponding gold standard (in red) in Figure 3(c3), which shows that both results are close to each other. As indicated by this comparison, our proposed framework can achieve satisfactory results.

Figure 4 demonstrates 6 example segmentation images during one heart beating cycle in the sixth series. The lateral walls of the RV are vague in these images, which is a normal phenomenon in the RV echocardiographic images that were affected by the lung or other structures. Even though, our automatic segmentation method still gave reasonable segmentation results. However, this poor imaging qualities of the RV images, especially at the lateral walls that entirely disappeared in some images (Figure 4), increased the disagreements between the auto-segmentation results and the manual ones.

4. DISCUSSION AND CONCLUSION

This study developed and evaluated an automatic segmentation framework for right ventricle ultrasound images. The segmentation method can automatically segment both

epicardial and endocardial boundaries from a continuous echocardiography series by combining sparse matrix transform, a training model, and a level set algorithm. Sparse matrix transform was applied to extract the eigenimages of current segmented echocardiograph series to automatically identify the RV location. Based on the extracted eigenimages, an RV training model is used as the initialization for a localized region based level set segmentation. Experimental results from human subject data validated the performance of the proposed framework in segmenting right ventricle from echocardiography.

Acknowledgments

This research is supported in part by NIH grant R01CA156775 (PI: Fei), Georgia Cancer Coalition Distinguished Clinicians and Scientists Award (PI: Fei), and the Emory Molecular and Translational Imaging Center (NIH P50CA128301).

REFERENCES

1. Noble JA, Boukerroui D. Ultrasound image segmentation: a survey. IEEE Trans Med Imaging. 2006; 25(8):987–1010. [PubMed: 16894993]
2. Chen YM, Tagare HD, Thiruvenkadam S, et al. Using prior shapes in geometric active contours in a variational framework. International Journal of Computer Vision. 2002; 50(3):315–328.
3. Taron M, Paragios N, Jolly MP. Border detection on short axis echocardiographic views using a region based ellipse-driven framework. Medical Image Computing and Computer-Assisted Intervention - MICCAI 2004, Pt 1, Proceedings. 2004; 3216:443–450.
4. Zhu Y, Papademetris X, Sinusas AJ, et al. A coupled deformable model for tracking myocardial borders from real-time echocardiography using an incompressibility constraint. Medical Image Analysis. 2010; 14(3):429–448. [PubMed: 20350833]
5. Dietenbeck T, Alessandrini M, Barbosa D, et al. Detection of the whole myocardium in 2D-echocardiography for multiple orientations using a geometrically constrained level-set. Medical Image Analysis. 2012; 16:386–401. [PubMed: 22119489]
6. Bosch JG, Mitchell SC, Lelieveldt BPF, et al. Automatic segmentation of echocardiographic sequences by active appearance motion models. IEEE Transactions on Medical Imaging. 2002; 21(11):1374–1383. [PubMed: 12575874]
7. Paragios N, Jolly MP, Taron M, et al. Active shape models and segmentation of the left ventricle in echocardiography. Scale Space and Pde Methods in Computer Vision Proceedings. 2005; 3459:31.
8. Zhou XS, Comaniciu D, Xie B, et al. A unified framework for uncertainty propagation in automatic shape tracking. Proceedings of the 2004 IEEE Computer Society Conference on Computer Vision and Pattern Recognition. 2004; 1:872–879.
9. Pearlman PC, Tagare HD, Lin BA, et al. Segmentation of 3D radio frequency echocardiography using a spatio-temporal predictor. Medical Image Analysis. 2012; 16(2):351–360. [PubMed: 22078842]
10. Cao GZ, Bachega LR, Bouman CA. The Sparse Matrix Transform for Covariance Estimation and Analysis of High Dimensional Signals. IEEE Transactions on Image Processing. 2011; 20(3):625–640. [PubMed: 20813641]
11. Bachega LR, Cao GZ, Bouman CA. Fast Signal Analysis and Decomposition on Graphs Using the Sparse Matrix Transform. IEEE International Conference on Acoustics Speech and Signal Processing. 2010:5426–5429.
12. Yang X, Akbari H, Halig L, Fei BW. 3D non-rigid registration using surface and local salient features for transrectal ultrasound image-guided prostate biopsy. Proceedings of SPIE. 2011; 7964:79642V.
13. Yang X, Fei BW. 3D Prostate Segmentation of Ultrasound Images Combining Longitudinal Image Registration and Machine Learning. Proceedings of SPIE. 2012; 8316:83162O-1.
14. Li K, Fei BW. A deformable model-based minimal path segmentation method for kidney MR images. Proceedings of SPIE. 2008; 6914:69144F-1.

15. Akbari H, Fei BW. 3D ultrasound image segmentation using wavelet support vector machines. Medical Physics. 2012; 39(6):2972–2984. [PubMed: 22755682]
16. Lankton S, Tannenbaum A. Localizing Region-Based Active Contours. IEEE Transactions on Image Processing. 2008; 17(11):2029–2039. [PubMed: 18854247]
17. Yang X, Fei BW. An MR brain classification method based on multiscale and multiblock fuzzy C-means. Medical Physics. 2011; 38:2879–2891. [PubMed: 21815363]
18. Wang H, Fei BW. A modified fuzzy C-means classification method using a multiscale diffusion filtering scheme. Medical Image Analysis. 2009; 13:193–202. [PubMed: 18684658]
19. Wang H, Feyes DK, Mulvihill JW, Oleinick NL, MacLennan G, Fei BW. Multiscale fuzzy C-means image classification for multiple weighted MR images for the assessment of photodynamic therapy in mice. Proceedings of SPIE. 2007; 6512:65122W-1.
20. Yang X, Wu S, Sechopoulos I, Fei BW. Cupping artifact correction and automated classification for high-resolution dedicated breast CT images. Medical Physics. 2012; 39:6397–6406. [PubMed: 23039675]
21. Fei BW, Lee Z, Boll DT, et al. Image registration and fusion for interventional MRI-guided thermal ablation of the prostate cancer. The Sixth Annual International Conference on Medical Imaging Computing and Computer Assisted Intervention (MICCAI) ***Lecture Notes in Computer Science (LNCS) Springer-VerlagBerlin Heidelberg. 2003; 2879:364–372.
22. Fei, BW.; Lee, Z.; Duerk, JL.; Wilson, DL. Image Registration for interventional MRI-guided procedures: similarity measurements, interpolation methods, and applications to the prostate. The Second International Workshop on Biomedical Image Registration Lecture Notes in Computer Science (LNCS) Springer-Verlag; Berlin Heidelberg. 2003. p. 321-329.
23. Wang H, Fei BW. An MR image-guided, voxel-based partialvolume correction method for PET images. Medical Physics. 2012; 39:179–195. [PubMed: 22225287]
24. Fei BW, Yang X, Nye JA, et al. MR/PET quantification tools: Registration, segmentation, classification, and MR-based attenuation correction. Medical Physics. 2012; 39:6443–6454. [PubMed: 23039679]
25. Akbari H, Fei BW. 3D ultrasound image segmentation using wavelet support vector machines. Medical Physics. 2012; 39:2972–2984. [PubMed: 22755682]
26. Akbari H, HaligL LV, Schuster DM, Osunkoya A, Master VA, Nieh PT, Chen GZ, Fei FW. Hyperspectral imaging and quantitative analysis for prostate cancer detection. Journal of Biomedical Optics. 2012; 17:076005. [PubMed: 22894488]

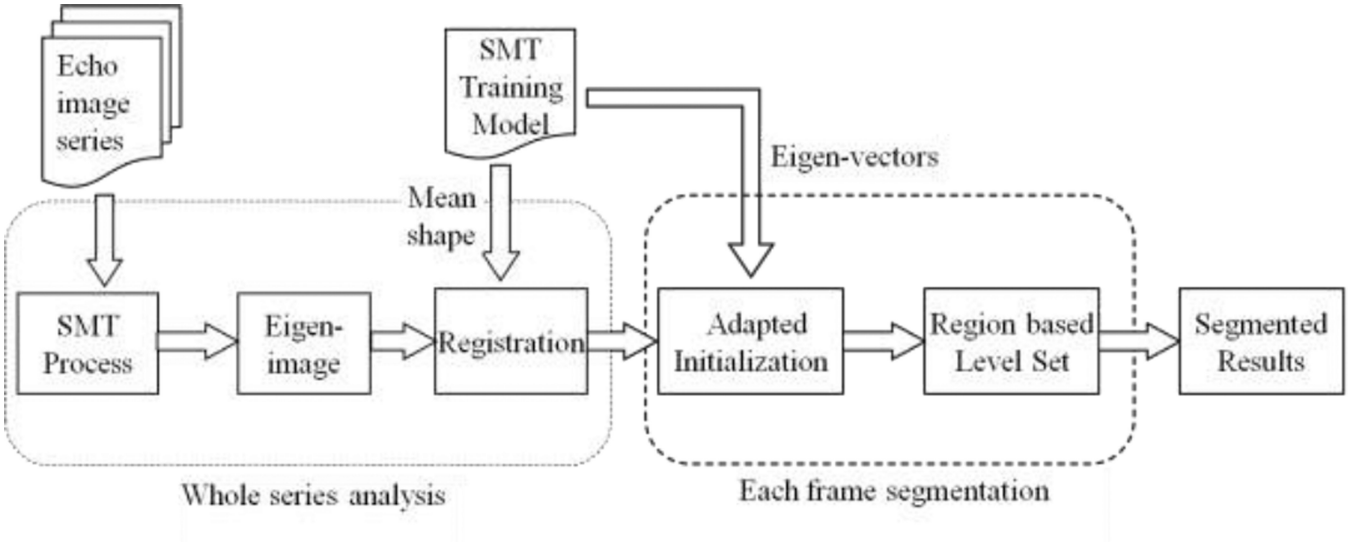

Figure 1.
Flowchart of the automatic ultrasound segmentation framework.

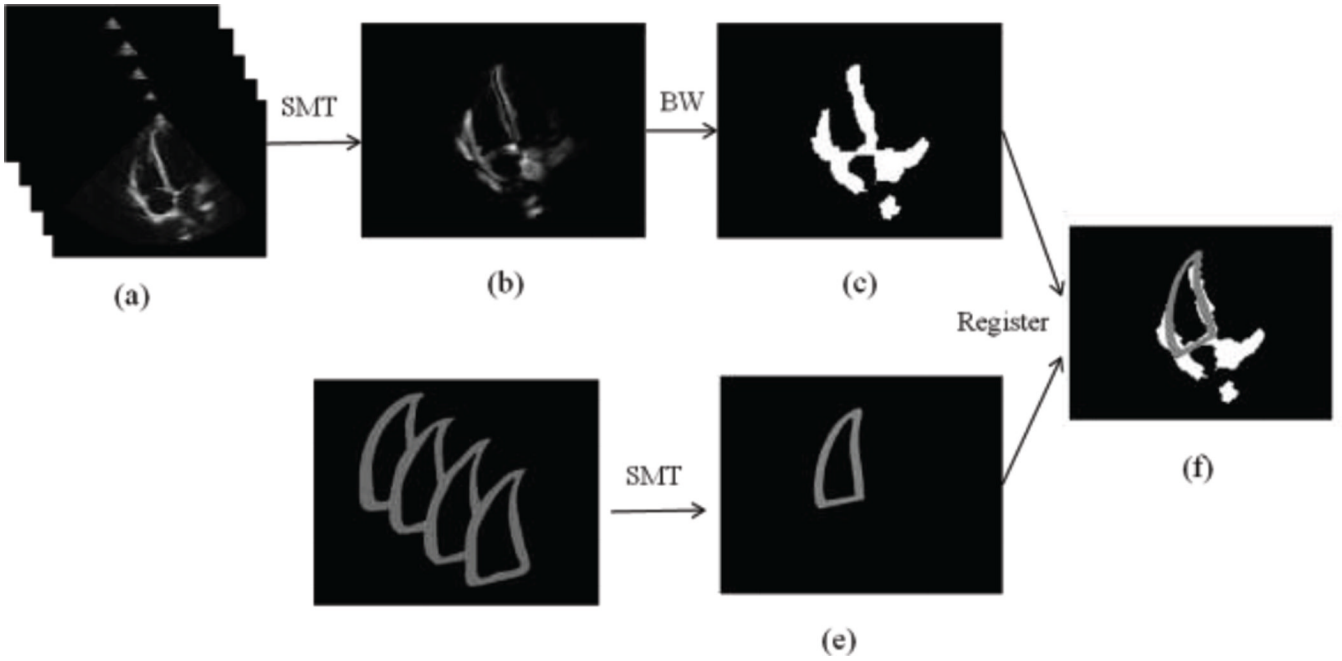

Figure 2.
The sparse matrix transform (SMT) eigenimages of one ultrasound series. (a) Ultrasound image series. (b) The combination of first 20 eigenimages extracted by SMT. (c) Corresponding black-white (BW) image of (b), where the white region indicates the most probable motion region of the myocardium. (d) Training data by manual segmentation. (e) Mean shape of the training model. (f) The registration result of the training model and the SMT eigenimages.

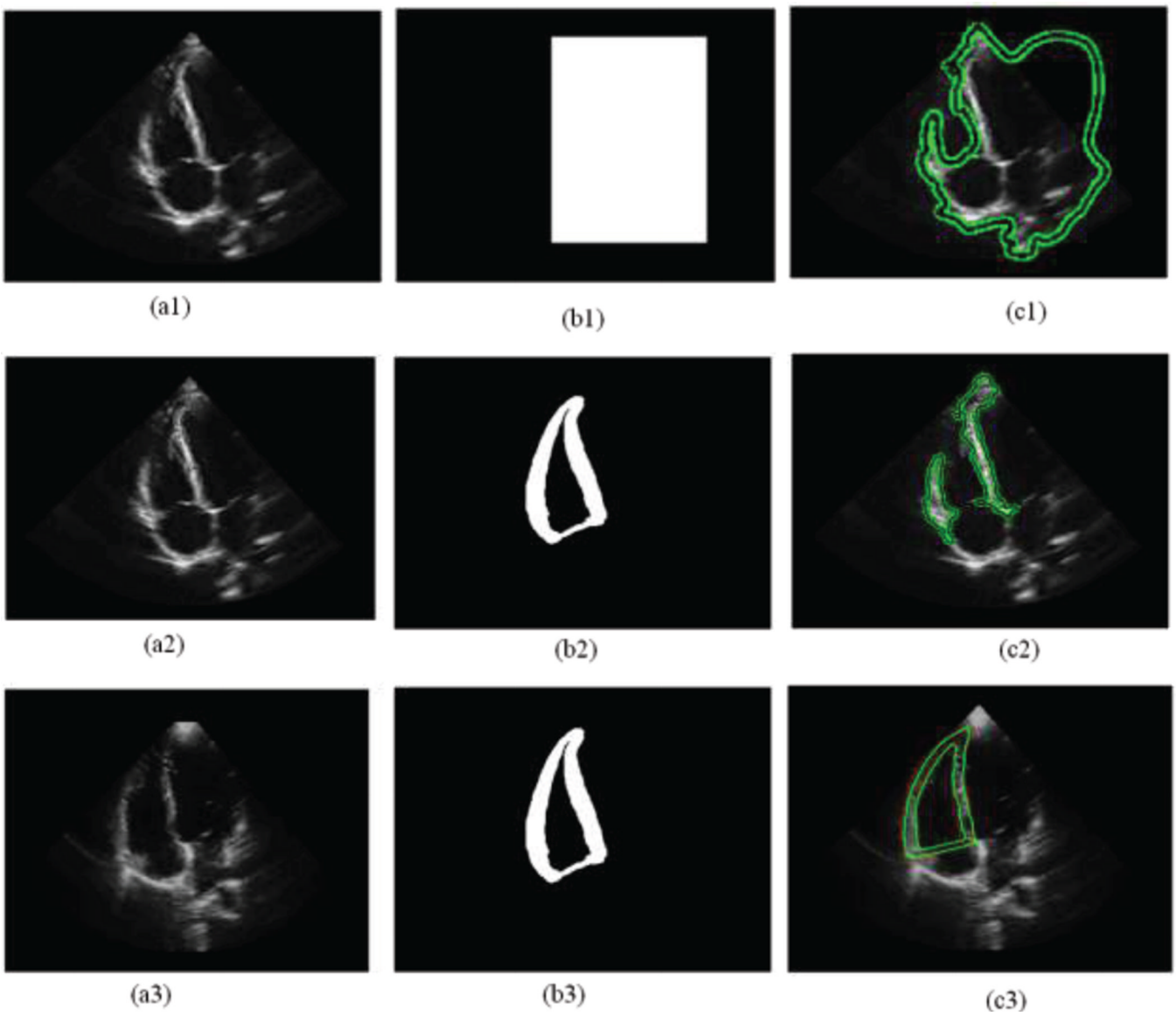

Figure 3.

The results segmented by different frameworks, where the green solid lines are the detected boundaries of myocardium. (c1) is the result of image (a1) segmented by the localized region based level set with the general initialization mask (b1) only. (c2) is the result of image (a2) segmented by the localized region based level set with an adapted initialization mask (b2) but without any restriction. (c3) is the result of image (a3) segmented by the localized region based level set with an adapted initialization mask (b3) and also restricted by the mask, where the red solid lines are its corresponding gold standard.

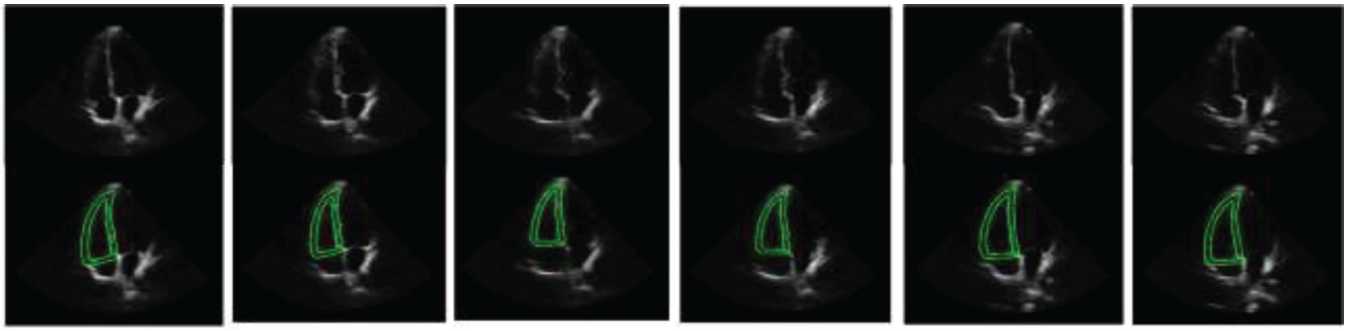

Figure 4.
Segmentation results during one heart beating cycle in the sixth series. The green lines segment both epicardial and endocardial boundaries of the RV. Note that the lateral wall of the RV is not clear on the image and it is challenging to segment the boundary.

Table 1

Endocardial (ENDO) and epicardial (EPI) Dice evaluation results

DICE	Series 1	Series 2	Series 3	Series 4	Series 5	Series 6	Series 7	Series 8
EPI Mean±STD (%)	88.8±2.2	92.5±2.4	88.3±3.1	91.8±1.9	88.6±3.6	87.3±3.8	88.1±2.6	87.2±3.6
ENDO Mean±STD (%)	83.0±7.2	88.6±5.1	81.2±8.2	86.6±6.4	81.9±9.0	80.3±8.8	86.2±6.5	81.0±7.8